UC Riverside

UC Riverside Previously Published Works

Title

Alterations of Parenchymal Microstructure, Neuronal Connectivity, and Cerebrovascular Resistance at Adolescence after Mild-to-Moderate Traumatic Brain Injury in Early Development

Permalink

https://escholarship.org/uc/item/18s8945f

Journal

Journal of Neurotrauma, 36(4)

ISSN

0897-7151

Authors

Parent, Maxime
Li, Ying
Santhakumar, Vijayalakshmi
et al.

Publication Date

2019-02-15

DOI

10.1089/neu.2018.5741

Peer reviewed

eScholarship.org Powered by the California Digital Library
University of California

JOURNAL OF NEUROTRAUMA 36:601–608 (February 15, 2019)
© Mary Ann Liebert, Inc.
DOI: 10.1089/neu.2018.5741

Alterations of Parenchymal Microstructure, Neuronal Connectivity, and Cerebrovascular Resistance at Adolescence after Mild-to-Moderate Traumatic Brain Injury in Early Development

Maxime Parent,[1] Ying Li,[2] Vijayalakshmi Santhakumar,[2,3] Fahmeed Hyder,[1,4] Basavaraju G. Sanganahalli,[1] and Sridhar S. Kannurpatti[5]

Abstract

Traumatic brain injury (TBI) is a leading cause of morbidity in children. To investigate outcome of early developmental TBI during adolescence, a rat model of fluid percussion injury was developed, where previous work reported deficits in sensorimotor behavior and cortical blood flow at adolescence.[1] Based on the nonlocalized outcome, we hypothesized that multiple neurophysiological components of brain function, namely neuronal connectivity, synapse/axonal microstructural integrity, and neurovascular function, are altered and magnetic resonance imaging (MRI) methods could be used to determine regional alterations. Adolescent outcomes of developmental TBI were studied 2 months after injury, using functional MRI (fMRI) and diffusion tensor imaging (DTI). fMRI-based resting-state functional connectivity (RSFC), representing neural connectivity, was significantly altered between sham and TBI. RSFC strength decreased in the cortex, hippocampus, and thalamus, accompanied by decrease in spatial extent of their corresponding RSFC networks and interhemispheric asymmetry. Cerebrovascular reactivity to arterial CO_2 changes diminished after TBI across both hemispheres, with a more pronounced decrease in the ipsilateral hippocampus, thalamus, and motor cortex. DTI measures of fractional anisotropy and apparent diffusion coefficient, reporting on axonal and microstructural integrity of the brain, indicated similar interhemispheric asymmetry, with highest change in the ipsilateral hippocampus and regions adjoining the ipsilateral thalamus, hypothalamus, and amygdala. TBI-induced corpus callosal microstructural alterations indicated measurable changes in interhemispheric structural connectivity. Hippocampus, thalamus, and select cortical regions were most consistently affected in multiple imaging markers. The multi-modal MRI results demonstrate cortical and subcortical alterations in neural connectivity, cerebrovascular resistance, and parenchymal microstructure in the adolescent brain, indicating the highly diffuse and persistent nature of the lateral fluid percussion TBI early in development.

Keywords: adolescence; cerebrovascular; connectivity; fMRI; traumatic brain injury

Introduction

A majority of traumatic brain injuries (TBI) are within a mild-to-moderate range of intensity, where patients mostly survive but suffer from morbidities such as mood disorders, cognitive deficits, post-traumatic epilepsy,[2–5] chronic neurodegenerative disease,[6] and accelerated aging.[7] TBI outcomes in the developing brain have distinct neural and cerebrovascular patterns[8] and higher susceptibility to excitotoxic secondary injury attributed to prominent excitatory neurotransmission and more intense cerebrovascular failure.[9–12] TBI pathology affects multiple components of the brain—including microstructural integrity, myelination, neural connectivity, and cerebrovascular functions[13]—with its myriad neurological and psychiatric morbidities.[2] As the neurobiological, cellular, and molecular basis of TBI pathology, including the milder and moderate forms that have emerged,[5,14–17] there is a need to take a systems approach and integrate these foundational studies with brain imaging to enhance potential for human

[1]Department of Radiology and Biomedical Imaging, Yale University School of Medicine, New Haven, Connecticut.
[2]Department of Pharmacology, Physiology and Neuroscience, Rutgers Biomedical and Health Sciences–New Jersey Medical School, Newark, New Jersey.
[3]Department of Molecular, Cell and Systems Neuroscience, University of California at Riverside, Riverside, California.
[4]Department of Biomedical Engineering, Yale University, New Haven, Connecticut.
[5]Department of Radiology, Rutgers Biomedical and Health Sciences–New Jersey Medical School, Newark, New Jersey.

translation.[18] Success of this integrative approach can lead to sophisticated imaging tools, where magnetic resonance imaging (MRI) is a leading candidate because of its translatability for inclusion in clinical diagnostic procedures for TBI patients.[19]

MRI-based translational imaging is widely applied in clinical TBI research. Early-stage (days to a few weeks after TBI) MRI of tissue structure has been shown to be valuable predictors of late-stage outcomes in humans.[20] Although pre-clinical and clinical functional MRI (fMRI) methods in the resting-state,[21–26] and task conditions[24,27–32] are well established in systems neuroscience assessments of brain function, resting-state fMRI and task fMRI studies are also currently valuable for human TBI research.[19,20,33–35] Pre-clinical MRI and fMRI applications related to TBI are increasingly applied because of the advent of longitudinal scans, suggesting systems-level outcome assessments for clinical translation.[36–39] However, MRI studies of TBI have rarely measured all the relevant neurophysiological components like parenchymal integrity, neural network connectivity, and cerebrovascular function simultaneously. Further, as TBI outcomes change during the developmental stages, there is a need to identify the evolution of morphological and functional components underlying developmental plasticity at critical stages of development, including adolescence.

Our previous studies on adolescent outcomes of the mild-to-moderate lateral fluid percussion TBI model during early development indicated persistent sensorimotor behavioral debilitation, accompanied by decreased ipsilateral baseline cerebral blood flow (CBF) and altered spatiotemporal CBF response to somatosensory stimuli in brain regions distant to the injury site.[1] The nonlocalized nature of the adolescent-stage brain functional changes after TBI at early development led us to hypothesize that functional and morphological components of brain function, namely neural connectivity, synapse/axonal microstructural integrity, and neurovascular function, are altered. In this study, we tested this hypothesis in a rat model of TBI (injury at P31), corresponding to approximately 2–4 years of human age,[40] and using fMRI and diffusion tensor imaging (DTI) at adolescence (2 months after injury) translating to approximately 12–14 years of human age.[40,41]

Regional morphological and functional changes characterized the pathological alterations in adolescent rats with early developmental TBI. Based on the multi-modal MRI approach and translatable task design of concurrently measuring clinically relevant outcomes, such as brain morphology, neural functional connectivity, and cerebrovascular integrity, clinical management of children and adolescents with past TBI may benefit from similar markers of outcome from pre-clinical animal models.

Methods

Animals

Male Sprague–Dawley rats (23–24 days old; weighing 60–80 g) were procured from Charles River Laboratories (Wilmington, MA). Rats were housed in pairs under controlled conditions and used for experiments after 30 days of age. All procedures were carried out in accord with the institutional guidelines and approved by the Institutional Animal Care and Use Committee of Rutgers Biomedical and Health Sciences–New Jersey Medical School (Newark, NJ).

Lateral fluid-percussion injury

Rats (age, P31) were subject to lateral fluid percussion injury (FPI) as previously described.[15,42] The FPI method produced diffuse moderate TBI. Briefly, animals were anesthetized with ketamine (80 mg/kg intraperitoneally [i.p.]) and xylazine (10 mg/kg i.p.) and positioned on a stereotaxic frame after confirming surgical plane anesthesia. A 3-mm craniotomy was performed on the left side of the skull −5 mm posterior to the bregma and 3 mm lateral to the sagittal suture while retaining the dura. A Luer–Lock syringe hub was glued surrounding the exposed dura using a cyanoacrylate adhesive. After 24 h, injury was induced to the TBI group ($n = 9$) by attaching the Luer–Lock hub of each isoflurane-anesthetized animal to the FPI device (Virginia Commonwealth University, Richmond, VA). A pendulum drop delivered a brief 20-ms impact on the intact dura. Impact pressure was measured by an extracranial transducer and controlled between 1.8 and 2.0 atmospheres. For the sham group ($n = 8$), animals underwent surgery to implant the hub and were isoflurane anesthetized and attached to the FPI device without the pendulum drop. Immediate neurological parameters, such as apnea, startle, and seizure-like behavior, were assessed within the first few minutes after injury. Sham and injured animals were subsequently monitored for the next 1 h and returned to their housing environment and monitored on a daily basis. One week after injury, animals were briefly anesthetized with isoflurane (1.5–2.0%) and the Luer–Lock hub was gently removed by twisting and the scalp was closed. Scalp incisions were completely healed by 3 weeks after injury over all animals.

Magnetic resonance imaging

MRI experiments were performed at adolescence (2 months after TBI). Animals were anesthetized using i.p. injection of urethane (1.3 mg/kg body weight), then placed in a custom-built frame, where they were freely breathing a mixture of O_2 and N_2O (30/70%) through a nose cone. Body temperature was monitored throughout the procedure using a rectal probe and maintained within 35–37°C using warm water pumped through a pad.

MRI data were obtained on a modified 9.4 Tesla system with a Bruker spectrometer (Bruker, Karlsruhe, Germany) and custom-built ^{1}H ellipsoidal surface coil (5×3 cm). Images were acquired over 12 contiguous coronal slices (thickness = 1 mm), covering the parenchyma between the olfactory bulb and cerebellum, with an in-plane field of view of 3.2×1.6 cm. Anatomical reference images (repetition time [TR]/echo time [TE] = 4000/30 ms, two averages) were acquired in a 128×64 matrix, for an effective in-plane resolution of 250×250 μm. Diffusion-sensitive images for DTI (TR/TE = 4000/20 ms, for averages) were acquired as a four-segment echo planar imaging (EPI) in a 64×32 matrix (in-plane resolution = 500×500 μm), with five A_0 images, 30 diffusion directions, and a b-value of 1000 s/mm^2. fMRI images using the EPI sequence (TR/TE = 1000/15 ms, preceded by eight dummy scans) were acquired with the same geometry as DTI: For the resting-state paradigm, each scan lasted for 5 min (300 repetitions), repeated four times per animal; the arterial CO_2 change-induced cerebrovascular reactivity functional scans lasted for 12 min (720 repetitions), with 10% CO_2 added to the breathing gas mixture between minutes 3 and 6 of the acquisition, and repeated twice per animal. Last, a fast three-dimensional (3D) anatomical scan (TR/TE = 50/5.6 ms, FA = 20 degrees, two averages) was acquired with an isotropic resolution of 250 μm, for image registration purposes.

Statistical analysis

Using BioImage Suite (http://bioimagesuite.yale.edu/), the tensor model was fitted at every voxel of the diffusion-sensitive images to generate parametric maps of fractional anisotropy (FA) and the three eigenvalues were averaged to obtain apparent diffusion coefficient (ADC) maps as described in our earlier studies.[43]

Using Analysis of Functional Neuro Image (AFNI) software,[44] functional images of CO_2 challenge were corrected for motion and spatially smoothed using a Gaussian filter (full width at half

maximum FWHM = 1.5 mm). Parametric maps of cerebrovascular reactivity (CVR) were generated from a voxel-level linear model and expressed as the *t*-statistical value of the contrast between baseline (frames 1–180) and CO_2 challenge (frames 210–360). For resting-state functional connectivity (RSFC) analysis, images were pre-processed and corrected for slice time and motion. Subsequently, images were linearly detrended, band-pass filtered (0.01–0.15 Hz), and spatially smoothed using a Gaussian filter (FWHM = 1.5 mm). Six seed voxels were randomly placed on the right (contralateral to the injury) sensorimotor cortex, hippocampus, and thalamus with the regions identified according to the rat brain atlas.[45] The signal time series from each selected random seed was cross-correlated with the entire brain producing six correlation maps each for the sensorimotor, hippocampal, and thalamic region seeds as demonstrated in our earlier studies. [46] Voxel-level correlation maps obtained with the six seed voxels were averaged in each animal and subsequently across animals in each group after Fisher z-transformation to generate group-level average RSFC maps. Voxels with average Pearson correlation coefficients (cc) >0.2 in clusters of at least 30 mm^3, corresponding to a corrected $p < 0.05$, represented active voxels of the respective RSFC network.

3D anatomical images were used to generate a nonlinear transform from each animal subject's native space to a common standard space, consisting of an averaged brain from all sham animals. The transform was then applied to all parametric maps of FA, ADC, CVR, and RSFC networks. Regions of interest (ROIs), which included the cortex, hippocampus, corpus callosum, internal capsule, and cingulum, were drawn on the common anatomical template of co-registered average brains from sham group identified using the rat brain atlas.[45]

Group contrasts were calculated from co-registered images with a voxel-level linear model for each modality, and significant differences were determined between sham and TBI groups using a two-tailed *t*-test with an adjusted threshold of $p < 0.05$ corrected for multiple comparisons using a random field theory approach.[47] Significantly different voxels were depicted as a color overlay on the anatomical image. Between-hemisphere differences were tested for asymmetry using the two-tailed *t*-test of the mean values from corresponding ROIs across each hemisphere in both sham and TBI groups.

Results

Sham animals did not show any immediate neurological signs, such as apnea, startle, or seizure-like behavior, whereas TBI animals displayed 6 ± 3 sec of apnea starting from the pendulum drop, startle in 6 of 9 animals, and seizure-like behavior in 1 of 9 animals.

Adolescent-stage T2-weighted gradient-echo–based structural MRI of the brain in TBI rats revealed no gross abnormality (Figure 1A); however, structurally hyperintense regions surrounding the FPI site were evident in T2-weighted spin echo images (Fig. 1A; arrow). Microstructural changes after TBI were determined by DTI measures of FA and ADC maps, indicators of myelin degeneration, cytoskeletal damage, and cellular integrity.[48–50] In the blinded analysis, sham or TBI animal subjects could be clearly distinguished on the basis of gross changes in FA in DTI data (Fig. 1A). One of the investigators (M.P.) was blind to the experimental groups during the performance of the MRI measurements and initial MRI data analysis. The experimental groups (e.g., sham or TBI) were revealed later to the blinded investigator for predictive accuracy determination and subsequent group analysis of the imaging data. One hundred percent prediction accuracy was achieved by the blinded investigator using T2-weighted spin echo images and DTI data, respectively, whereas only 70% prediction accuracy could be achieved using T2-weighted gradient-echo–based MR images. Subsequent unblinded comparison of DTI

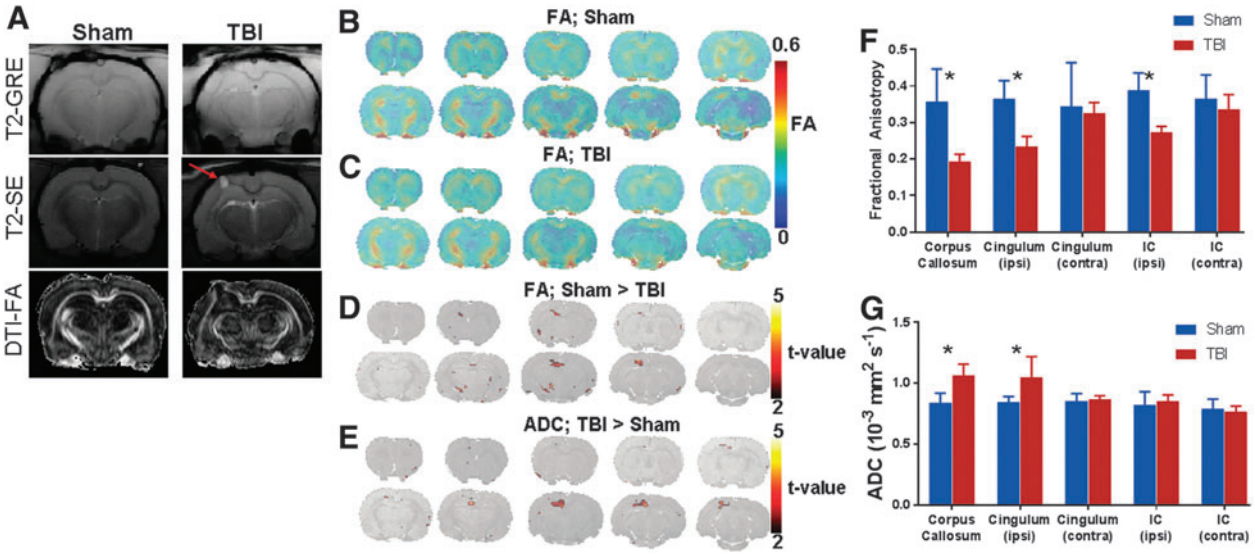

FIG. 1. (**A**) Typical T2-weighted gradient echo (GRE), spin echo (SE), and fractional anisotropy (FA) images obtained from diffusion tensor imaging (DTI) of sham and TBI animal. The mild-to-moderate intensity fluid percussion TBI impact region was clearly identified in T2-weighted anatomical SE image and DTI-FA images, respectively (arrows), but not apparent in the T2-weighted GRE image. (**B**) Group average FA-sham ($n = 8$), (**C**) Group average FA-TBI ($n = 9$). (**D**) FA (sham > TBI) and (**E**) apparent diffusion coefficient (ADC; sham > TBI). Significant difference determined by a two-way *t*-test corrected for multiple comparisons between sham and TBI groups. Voxels with t-values >2; corresponding to a corrected $p < 0.05$ are significantly different sham versus TBI (depicted by the color statistical overlay on the anatomical image). ROIs in the corpus callosum, cingulum, and internal capsule (IC) were used to average group-level parameters of (**F**) FA and (**G**) ADC. Significant TBI-induced microstructural changes were observed mostly in the corpus callosum and ipsilaterally in the cingulum and internal capsule (IC); $^*p < 0.01$; two tailed *t*-test. ROIs, regions of interest; TBI, traumatic brain injury.

parametric maps from sham and TBI groups revealed a significant reduction in FA and increased ADC in the ipsilateral and interhemispheric fibers of injured rat brains compared to sham (Fig. 1D,E). Diffusion-related changes were apparent in the corpus callosum, ipsilateral hippocampus, and regions adjoining the hypothalamus (Fig. 1D,E). Bilateral FA changes were also observed in the S1/S2 somatosensory and entorhinal cortices (Fig. 1D). Corpus callosum showed significantly lower FA values in TBI when compared to sham (Fig. 1F). Significantly lower FA values were also observed in the ipsilateral cingulum and internal capsule (IC) ROIs in TBI when compared to sham (Fig. 1F), indicating sustained damage to fiber tracts or demyelination across the ipsilateral hemisphere after TBI. Relatively less-intense morphological changes were observed in the contralateral hemisphere in TBI when compared to sham (Fig. 1F). ADC values increased significantly in the same ROIs, with the exception of ipsilateral IC, indicating increased isotropic diffusion (Fig. 1G), and consistent with the decreased FA observed in these regions (Fig. 1F).

Given the widespread microstructural changes on either hemispheres and in interhemispheric connections, corresponding asymmetry in functional connectivity can be expected. To investigate this, fMRI-BOLD (blood level oxygen dependent) measurements in the resting state were performed to determine RSFC of different networks using seed voxels from different anatomical ROIs from the stereotaxic rat brain atlas,[45] as implemented in our earlier studies.[46,51] Somatosensory cortical, hippocampal, and thalamic RSFC networks were obtained by cross-correlating all brain voxels with the respective seeds from the contralateral sensorimotor cortical, hippocampal, and thalamic ROIs. All RSFC networks showed higher bilateral symmetry in sham compared to TBI animals (Fig. 2A–C). RSFC strength at the group level was determined from six RSFC maps obtained from cross-correlation with the six random seeds placed in the contralateral cortex, hippocampus, and thalamus after averaging in each animal and subsequently over all animals in the respective groups after z-transformation. The TBI group showed significantly reduced ipsilateral RSFC strength over the cortical, hippocampal, and thalamic ROIs compared to sham (Fig. 2D).

fMRI measures of arterial CO_2 change-induced CVR was obtained using a transient (3-min) inhalation of 10% CO_2 gas mixture to induce hypercapnia as a vasodilatory stimulus. CVR maps were obtained on a voxel-by-voxel basis based on fMRI-BOLD response amplitude to the CO_2 stimulus. Sham animals had a significantly higher global CVR response as observed by the t-values proportional to the relative signal enhancement of fMRI-BOLD between the normo- and hypercapnic states (Fig. 3A), when compared to

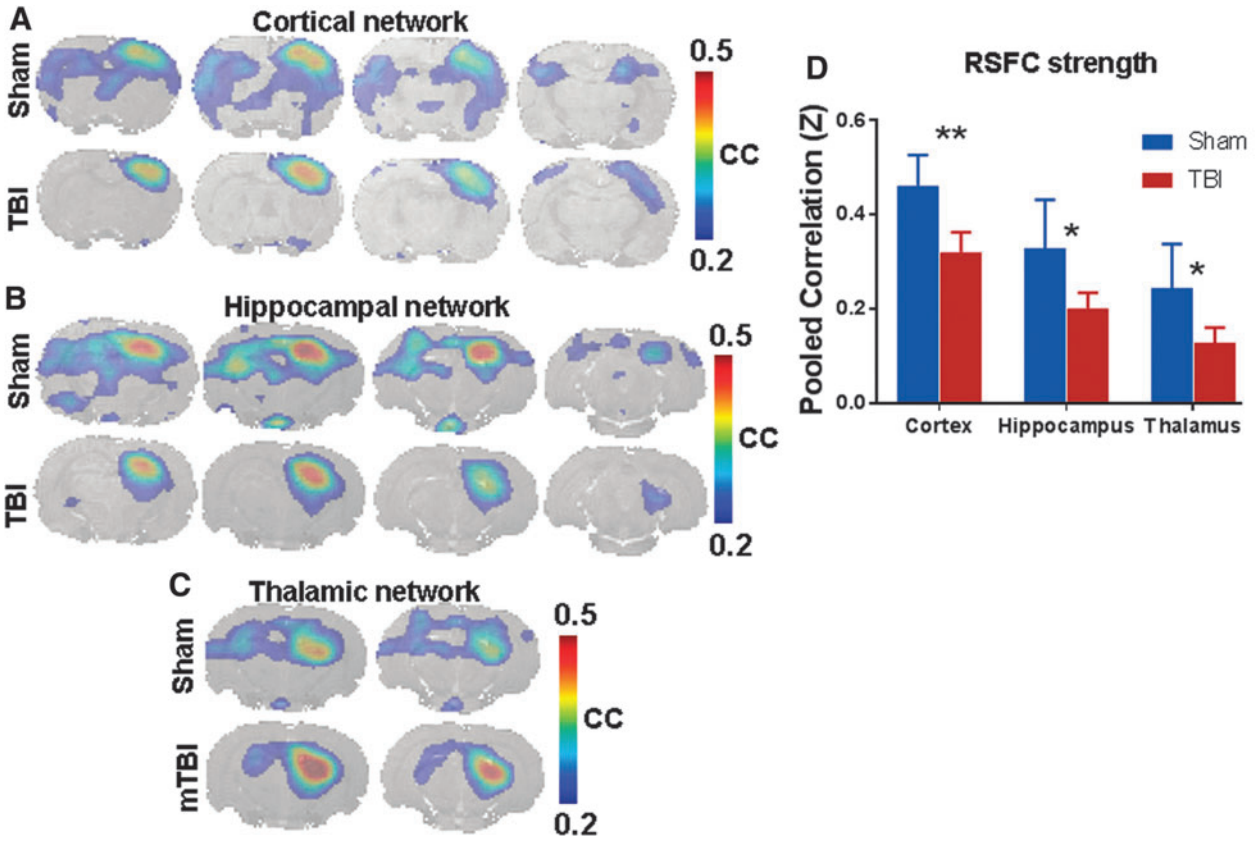

FIG. 2. Resting-state functional connectivity (RSFC) maps obtained for sham and TBI animals using seeds from different networks. RSFC maps were obtained from six right-hemisphere seeds placed in (**A**) somatosensory cortex, (**B**) hippocampus, and (**C**) thalamus and cross-correlating the seed voxel time series with the signal time series across all voxels in the brain and subsequently averaged after Fisher Z-transform. Voxels with average correlation coefficients (cc) >0.2; corresponding to a corrected $p < 0.05$ represent active voxels of the respective RSFC network. Interhemispheric symmetry in RSFC network topology was apparent with a large disruption in TBI. (**D**) RSFC strength determined after averaging the cc values from the cortical, hippocampal, and thalamic ROIs from either hemisphere in sham and TBI groups. Ipsilateral RSFC strength was significantly lower for TBI ($n = 9$) compared to sham ($n = 8$). $^{**}p < 0.01$; $^{*}p < 0.05$; two-tailed *t*-test. mTBI, mild TBI; ROIs, regions of interest; TBI, traumatic brain injury.

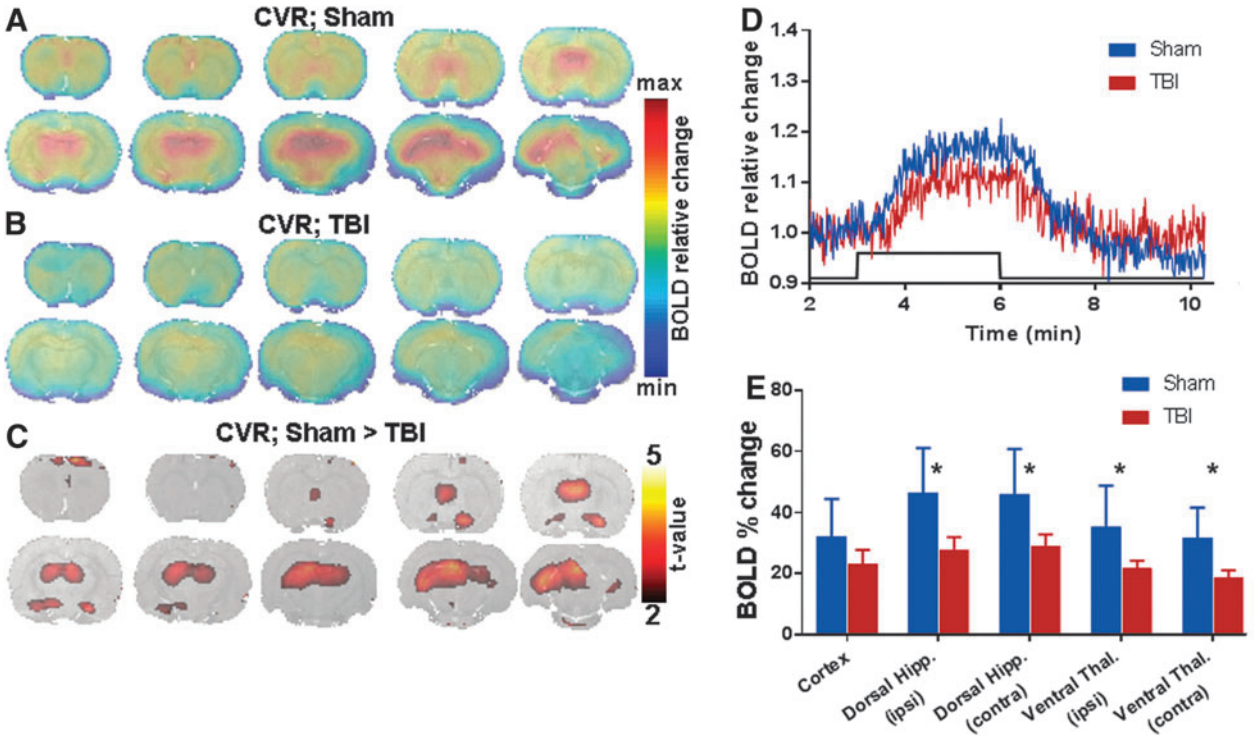

FIG. 3. Cerebrovascular reactivity (CVR) response to transient carbon dioxide inhalation in (**A**) sham ($n=8$), (**B**) TBI ($n=9$), and (**C**) significant difference in cerebrovascular reactivity determined by a two-way *t*-test corrected for multiple comparisons between sham and TBI groups. Voxels with t-value >2; corresponding to a corrected $p<0.05$ are significantly different sham versus TBI (depicted by the color statistical overlay on the anatomical image). (**D**) Typical sensorimotor cortex voxel time course of the BOLD signal in response to the transient 3-min CO_2 challenge (indicated by the back line step function) in a sham and TBI animal, respectively. (**E**) Group-level cerebrovascular reactivity (% change BOLD) from different ROIs showing significant ipsilateral cerebrovascular reactivity insufficiency across TBI animals. *$p<0.05$; two tailed *t*-test. ROIs, regions of interest; TBI, traumatic brain injury.

TBI (Fig. 3B). A group analysis was performed using a two-tailed *t*-test to test for voxel-wise CVR differences between sham and TBI groups. In TBI, CVR insufficiency encompassed the hippocampus thalamus and regions neighboring the amygdale with a predominant ipsilateral localization along with significant extension toward the contralateral hemisphere (Fig. 3C,E). However, CVR insufficiency was confined to only specific regions in the cortex with only the entorhinal and sensorimotor cortices affected on either hemisphere (Fig. 3C).

Discussion

The quest for novel treatments against TBI and their *in vivo* assessments may not only demand systems-level approaches,[18] but also additional abilities for seamless cross-comparison between pre-clinical and human studies using similar markers. Further, TBI pathology affects multiple components of the brain—including microstructural integrity, neuronal connectivity, and CVR.[13] The present study assessed the adolescent-stage impact of TBI sustained during early development using simultaneously assessed, clinically relevant, MRI-based brain morphological and functional markers.

The fluid percussion model produces a mixed form of local and diffuse injury in the brain.[1,16] Milder forms of concussive TBI in humans generally do not show structural lesions in MRI. Although in the current pre-clinical TBI model no specific injury induced lesion volume was detected from the T2-weighted gradient echo (GRE) images of the brain (Fig. 1A), T2-weighted spin echo (SE) images showed hyperintensity localized exclusively to the injury site without any perilesional effects. Hence, we categorized the present TBI model in the mild-to-moderate range based on the anatomical MRI results. Similar to concussive human TBI, diffusion-sensitive MRI contrast after tensor modeling detected further abnormalities not only in the lesion area (Fig. 1A), but also in several white-matter–rich structures throughout the brain, as demonstrated by the DTI-FA and DTI-ADC value differences between sham and TBI (Fig. 1D,E). Brain microstructural alterations were most prominent across the ipsilateral hippocampus, thalamus, cingulum, and IC, confirming the relatively higher impact of the lateralized TBI on the ipsilateral brain (Fig. 1F,G). DTI-FA and DTI-ADC value changes also occurred on the contralateral hemisphere, indicating the extensive and nonlocalized nature of parenchymal microstructural changes induced by the pre-clinical fluid percussion TBI model. Measurable alterations in interhemispheric structural connectivity could be ascertained from the DTI markers across the corpus callosum (Fig. 1F,G). The highly diffuse nature of the fluid percussion TBI on brain morphology at the adolescent stage with prominent alterations in brain interhemispheric structural connectivity and the specific regions affected parallel the diffuse morphological changes observed in pediatric and adolescent concussive injury patients.[52]

Neural activity in the resting-state brain represented by RSFC is a well-known marker of spontaneous neuronal activity.[21,22,25,46] Given that the TBI was lateralized, injury intensity is expected to be highest in the ipsilateral hemisphere with relatively lesser effect on the contralateral hemisphere. Our previous studies on the early

stages after developmental TBI (1–21 days after injury) indicated intense sensorimotor behavioral deficits accompanied by ipsilateral neurodegeneration.[1] Asymmetric brain spatiotemporal CBF responses to whisker-deflection stimuli was observed at adolescence (2 months post-TBI), with a significantly reduced ipsilateral CBF response and diffuse nonclusterized contralateral CBF response.[1] The current spontaneous neural activity of the brain represented by the RSFC network spatial extents and RSFC strength[46] suggested that neural connectivity was patently altered at adolescence after TBI during early development (Fig. 2). The current RSFC results, taken together with previous evidence of interhemispheric asymmetry in stimulus-induced activation of the adolescent brain,[1] suggest that both spontaneous and stimuli-induced activity in neural circuits are permanently altered at adolescence after developmental TBI. The highly disrupted ipsilateral neural functional connectivity may be a primary consequence of the early-stage (0–8 days) neuronal loss after TBI observed in this model.[16] An interhemispheric difference in neurodegeneration was also evident in the ipsilateral cortical and hippocampal areas as determined by histology at adolescence in our earlier study.[1] Additional factors, such as compromised axonal and synaptic functions within surviving neurons, astrocytes, and supporting vascular functions post-TBI, could also affect the overall neural functional connectivity.[13] Altered functional connectivity in specific networks, such as the motor network, has been correlated with poor performance in simple motor inhibitory and reward-related motivational behavior among adolescent TBI patients.[53] Fractal analysis of the resting-state fMRI signal in the whole brain in children (mean age of 13 years) with mild TBI show significant changes in amygdala, hypothalamus, hippocampus, vermis, and the caudate head,[54] confirming several earlier independent human studies implicating these regions in childhood concussive TBI.[52] However, brain connectivity studies using fMRI-based RSFC networks also showed significant alterations in the hippocampal and cortical networks along with interhemispheric disruptions in asymptomatic concussive TBI patients, cautioning the limitations of conventional clinical and neuropsychological examinations.[55] The current pre-clinical neural connectivity assessments, in this view, have a strong translational value in characterizing TBI outcome throughout development and into adolescence when behaviors change dynamically. Additionally, it also demonstrates the feasibility and potential utility of structural and functional brain mapping in behaviorally asymptomatic animal models of developmental TBI.

CBF decreases immediately post-TBI, including the milder forms, and continues to be depressed for long periods of time depending upon severity.[56] Insufficient CBF and oxygen delivery, critical for normal neurophysiological activity, may contribute to ischemic episodes and secondary injury.[57] This situation becomes unique as acute arterial CO_2 mediated cerebrovascular reactivity is impaired after TBI only in younger humans (age <30 years) with no effect on older subjects (age >30 years).[10] Animal models capture these cerebrovascular differences to a certain extent, where a transient increase in cerebral hemoglobin saturation (27%) followed by a profound decrease (45%) have been observed 30 sec after TBI in young piglets, but only a modest increase of 10% followed by a mild decrease of 4% in adolescent animals.[9] Whereas developmental TBI is unique in its cerebrovascular outcome, the current results highlight the persistent CVR deficiencies at adolescence after an early-development TBI. The prolonged CVR impairment demonstrated in this milder form of TBI during early development suggests that it may be a significant contributor to altered brain function and behavioral morbidities in TBI-afflicted children. Cerebrovascular deficiencies were most intense in the deeper subcortical regions despite the injury site directed at the cortex, which suggests that significant cerebrovascular repair/rearrangement occurred in the cortical and other areas with time. Chronic vascular rearrangements are known to occur after TBI.[58] Long-term follow-up of TBI in animal models (beyond 6 months after injury) show large-scale proliferation of blood vessels in both lesional and perilesional regions of the brain along with diverse vascular rearrangements, depending on the brain anatomical region.[58] Such differences in TBI-induced chronic cerebrovascular regeneration have been observed in adult rats along with behavioral ramifications.[58] The variable effect of TBI during early development on regional vascular rearrangement and function based on anatomical location observed in the current developmental TBI model are similar to adult animals.[58] CVR abnormalities were also pronounced in the hippocampus and thalamus of both hemispheres (Fig. 3C), accompanied by neural connectivity changes (Fig. 2B–D) and parenchymal microstructural changes (Fig. 1B–E), indicating that these regions with arterial CO_2-dependent CVR compromise may be at high risk of cerebrovascular insufficiency related to perfusion pressure and arterial oxygenation leading to chronic ischemic secondary neuronal injury/death attributed to mitochondrial dysfunction on the long term after TBI. These results parallel the hypoperfusion and low oxygen metabolic index observed in children 3 months after a severe TBI,[59] and suggests that a similar phenomenon may exist in milder forms of TBI as well and concentrated in the thalamic and hippocampal regions. The current MRI-based multi-modal markers have ramifications for the follow-up of TBI patients as arterial CO_2-mediated CVR can be assessed noninvasively in the clinic and may likely overlap with neural connectivity deficiencies and morphological changes where chronic secondary injury may be ongoing.

Neurodegenerative changes post-TBI are comparatively understudied in children, suggesting the need for animal model systems-level studies of long-term neurodegenerative changes using similar markers available in children and youth post-TBI.[52] Prominent fMRI/DTI-based studies of brain regions in children after concussive TBI show morphological changes in the hippocampus, thalamus, amygdala, hypothalamus, globus pallidus, periventricular white matter, brainstem, and corpus callosum.[52] Whereas neurodegeneration after TBI is hypothesized to be prominent in these selective regions of the developing brain, it persists on longer time scales through development and into adolescence. The pre-clinical results of the current study provide developmental TBI outcome markers, such as decrease in resting-state connectivity across cortical networks, reduced CVR, and specific parenchymal changes using fMRI/DTI with potential for improved clinical evaluation of adolescent TBI patients sustaining injury early in life.

Conclusions

The multi-modal MRI imaging results demonstrate TBI-induced changes in the adolescent brain. Decreases in neural connectivity across cortical, hippocampal, and thalamic resting-state functional connectivity networks were observed. TBI reduced CVR across both hemispheres, with a more pronounced decrease in the ipsilateral hippocampus, thalamus, and motor cortex. Parenchymal microstructural changes were prominent in the ipsilateral hippocampus and regions adjoining the ipsilateral thalamus, hypothalamus, and amygdala. Functional and morphological changes were observed across both hemispheres, with a relatively less-intense effect on the contralateral brain, indicating the highly diffuse and

persistent nature of the lateral fluid percussion TBI early in development. The whole-brain microstructural and functional alterations carried over into adolescence in the current TBI model corresponded with prominent human brain regions (e.g., hippocampus, thalamus, amygdala, hypothalamus, and corpus callosum) implicated in concussive TBI children.[52] Hippocampal and thalamic regions changing across all MRI markers suggest the vulnerability of these brain regions to further degeneration attributed to cerebrovascular insufficiency in the chronic phase after TBI.

Acknowledgments

Funding from the New Jersey Commission for Brain Injury research CBIR12PIL028 (S.K.), CBIR15IRG010 (S.K.), R01 NS097750 (V.S.), R01 MH-067528 (F.H.), and P30 NS-052519 (F.H.) are acknowledged.

Author Disclosure Statement

No competing financial interests exist.

References

1. Murugan, M., Santhakumar, V., and Kannurpatti, S. (2016). Facilitating mitochondrial calcium uptake improves activation-induced cerebral blood flow and behaviour after mTBI. Front. Neurosci. 10, 19.
2. Annegers, J.F., Grebow, J.D., Groover, R.D., Laws, E.R., Elveback, L.R., and Kurland, L.T. (1980). Seizures after head trauma—a population study. Neurology 30, 683–689.
3. Barlow, K.M., Spowart, J.J., and Minns, R.A. (2000). Early post-traumatic seizures in non-accidental head injury: relation to outcome. Dev. Med. Child Neurol. 42, 591–594.
4. Kharatishvili, I., Nissinen, J., and Pitkanen, A. (2005). Lateral fluid percussion injury in rat—a clinically relevant model of post-traumatic epilepsy. J. Neurotrauma 22, 1208.
5. Pitkänen, A., Kharatishvili, I., Nissinen, J., and McIntosh, T.K. (2006). Posttraumatic epilepsy induced by lateral fluid-percussion brain injury in rats, in: *Models of Seizures and Epilepsy*. Academic: New York, NY, pps. 465–476.
6. Chauhan, N. B. (2014). Chronic neurodegenerative consequences of traumatic brain injury. Restor. Neurol. Neuros. 32, 337–365.
7. Cole, J.H., Leech, R., Sharp, D.J.; Alzheimer's Disease Neuroimaging Initiative. (2015). Prediction of brain age suggests accelerated atrophy after traumatic brain injury. Ann. Neurol. **77**, 571–581.
8. Mannix, R., Berkner, J., Mei, Z.R., Alcon, S., Hashim, J., Robinson, S., Jantzie, L., Meehan, W.P., and Qiu, J.H. (2017). Adolescent mice demonstrate a distinct pattern of injury after repetitive mild traumatic brain injury. J. Neurotrauma 34, 495–504.
9. Armstead, W.M., Kurth, C.D. (1994). Different cerebral hemodynamic-responses following fluid percussion brain injury in the newborn and juvenile pig. J. Neurotrauma 11, 487–497.
10. Len, T.K., Neary, J.P. (2011). Cerebrovascular pathophysiology following mild traumatic brain injury. Clin. Physiol. Funct. Imaging 31, 85–93.
11. Mcdonald, J.W., Silverstein, F.S., Johnston, M.V. (1988). Neurotoxicity of N-methyl-D-aspartate is markedly enhanced in developing rat central nervous-system. Brain Res. 459, 200–203.
12. Mcdonald, J.W., Silverstein, F.S., Johnston, M.V. (1988). Developmental alteration in N-methyl-D-aspartate receptor channel binding characteristics and its relationship to neurotoxicity in immature brain. Ann. Neurol. 24, 337–337.
13. Park, E., Bell, J.D., Baker, A.J. (2008). Traumatic brain injury: can the consequences be stopped? Can. Med. Assoc. J. 178, 1163–1170.
14. Gao, X., and Chen, J. (2011). Mild traumatic brain injury results in extensive neuronal degeneration in the cerebral cortex. J. Neuropathol. Exp. Neurol. 70, 183–191.
15. Gupta, A., Elgammal, F.S., Proddutur, A., Shah, S., and Santhakumar, V. (2012). Decrease in tonic inhibition contributes to increase in dentate semilunar granule cell excitability after brain injury. J. Neurosci. 32, 2523–2537.
16. Lifshitz, J., and Lisembee, A.M. (2011). Neurodegeneration in the somatosensory cortex after experimental diffuse brain injury. Brain Struct. Funct. 217, 49–61.
17. Povlishock, J.T., and Christman, C.W. (1995). The pathobiology of traumatically induced axonal injury in animals and humans—a review of current thoughts. J. Neurotrauma 12, 555–564.
18. Chen, H.C.I., Burke, J.F., and Cohen, A.S. (2016). Editorial: traumatic brain injury as a systems neuroscience problem. Front. Syst. Neurosci. 10, 100.
19. Wintermark, M., Coombs, L., Druzgal, T.J., Field, A.S., Filippi, C.G., Hicks, R., Horton, R., Lui, Y.W., Law, M., Mukherjee, P., Norbash, A., Riedy, G., Sanelli, P.C., Stone, J., Sze, G., Tilkin, M., Whitlow, C.T., Wilde, E., York, G., Provenzale, J.M., and American College of Radiology Head Injury Institute. (2015). Traumatic brain injury imaging research roadmap. AJNR Am. J. Neuroradiol. 36, E12–E23.
20. Yuh, E.L., Uh, E.L., Mukherjee, P., Lingsma, H.F., Yue, J.K., Ferguson, A.R., Gordon, W.A., Valadka, A.P., Schnye, D.M., Okonkwo, D.O., Maas, A.I., Manley, G.I., and TRACK TBI Investigator. (2013). Magnetic resonance imaging improves 3-month outcome prediction in mild traumatic brain injury. Ann. Neurol. 73, 224–235.
21. Biswal, B., Yetkin, F.Z., Haughton, V.M., and Hyde, J.S. (1995). Functional connectivity in the motor cortex of resting human brain using echo-planar MRI. Magn. Reson. Med. 34, 537–541.
22. Biswal, B.B., and Kannurpatti, S.S. (2009). Resting-state functional connectivity in animal models: modulations by exsanguination. Methods Mol. Biol. 489, 255–274.
23. Buckner, R.L., Andrews-Hanna, J.R., and Schacter, D.L. (2008). The brain's default network: anatomy, function, and relevance to disease. Ann. N. Y. Acad. Sci. 1124, 1–38.
24. Kannurpatti, S.S., Motes, M.A., Rypma, B., and Biswal, B.B. (2011). Increasing measurement accuracy of age-related BOLD signal change: Minimizing vascular contributions by resting-state-fluctuation-of-amplitude scaling. Hum. Brain. Mapp. 32, 1125–1140.
25. Pawela, C.P., Biswal, B.B., Cho, Y.R., Kao, D.S., Li, R., Jones, S.R., Schulte, M.L., Matloub, H.S., Hudetz, A.G., and Hyde, J.S. (2008). Resting-state functional connectivity of the rat brain. Magn. Reson. Med. 59, 1021–1029.
26. Hyder, F. (2010). in: 2nd Biennial International Conference on Resting-State Functional Brain Connectivity, September 16–19, 2010, Milwaukee WI.
27. Bandettini, P.A., Wong, E.C., Hinks, R.S., Tikofsky, R.S., and Hyde, J.S. (1992). Time course EPI of human brain function during task activation. Magn. Reson. Med. 25, 390–397.
28. D'Esposito, M., Zarahn, E., Aguirre, G. K., and Rypma, B. (1999). The effect of normal aging on the coupling of neural activity to the bold hemodynamic response. Neuroimage 10, 6–14.
29. Harel, N., Lee, S.P., Nagaoka, T., Kim, D.S., and Kim, S.G. (2002). Origin of negative blood oxygenation level-dependent fMRI signals. J. Cereb. Blood Flow Metab. 22, 908–917.
30. Ogawa, S., Lee, T.M., Nayak, A.S., and Glynn, P. (1990). Oxygenation-sensitive contrast in magnetic resonance image of rodent brain at high magnetic fields. Magn. Reson. Med. 14, 68–78.
31. Sanganahalli, B.G., Herman, P., Hyder, F., and Kannurpatti, S.S. (2013). Mitochondrial calcium uptake capacity modulates neocortical excitability. J. Cereb. Blood Flow Metab. 33, 1115–1126.
32. Yang, X., Hyder, F., and Shulman, R.G. (1996). Activation of single whisker barrel in rat brain localized by functional magnetic resonance imaging. Proc. Natl. Acad. Sci. U. S. A. 93, 475–478.
33. Johnson, B., Zhang, K., Gay, M., Horovitz, S., Hallett, M., Sebastianelli, W., and Slobounov, S. (2012). Alteration of brain default network in subacute phase of injury in concussed individuals: resting-state fMRI study. Neuroimage 59, 511–518.
34. Lima, F.P., Lima, M.D., Leon, D., Lucareli, P.R., Falcon, C., Cogo, J.C., Bargalla, N., Vidal, J., Bernabeu, M., and Jongue, C. (2010). fMRI of the sensorimotor cortex in patients with traumatic brain injury after intensive rehabilitation. Neurol. Sci. 32, 633–639.
35. Slobounov, S.M., Zhang, K., Pennell, D., Ray, W., Johnson, B., and Sebationelli, W. (2010). Functional abnormalities in normally appearing athletes following mild traumatic brain injury: a functional MRI study. Exp. Brain Res. 202, 341–354.
36. Duong, T. (2015). MRI of experimental traumatic brain injury. J. Neurotrauma 32, A138.
37. Mishra, A.M., Bai, X.X., Sanganahalli, B.G., Waxman, S.G., Shatillo, O., Grohn, O., Hyder, F., and Pitkanen, A. (2014). Decreased resting

functional connectivity after traumatic brain injury in the rat. PLoS One 9, e95280.
38. Shen, Q., Watts, L.T., Li, W., and Duong, T.Q. (2016). Magnetic resonance imaging in experimental traumatic brain injury. Methods Mol Biol. 1462, 645–658.
39. Watts, L., Long, J., Shen, Q., and Duong, T. (2015). Neuroprotective effect of methylene blue in moderate traumatic brain injury. J. Neurotrauma 32, A48.
40. Clancy, B., Darlington, R.B., and Finlay, B.L. (2001). Translating developmental time across mammalian species. Neuroscience 105, 7–17.
41. Andreollo, N.A., Santos, E.F., Araujo, M.R., and Lopes, L.R. (2012). Rat's age versus human's age: what is the relationship? [Article in English, Portuguese]. Arq. Bras. Cir. Dig. 25, 49–51.
42. Li, Y. Korgaon, A.A., Swietek, B., Wang, J., Elgammal, F.S., Elkabes, S., and Santhakumar, V. (2015). Toll-like receptor 4 enhancement of non-NMDA synaptic currents increases dentate excitability after brain injury. Neurobiol. Dis. 74, 240–253.
43. Kaneko, G. Sanganahalli, B.G., Groman, S.M., Wang, H., Canan, D., Rao, J., Herman, P., Jiang, L., Rich, K., de Graaf, R.A., Taylor, J.R., and Hyder, F. (2017). Hypofrontality and posterior hyperactivity in early schizophrenia: imaging and behavior in a preclinical model. Biol. Psychiatry 81, 503–513.
44. Cox, R.W. (1996). AFNI: software for analysis and visualization of functional magnetic resonance neuroimages. Comput. Biomed. Res. 29, 162–173.
45. Paxinos, G. & Watson, C. (1998). *The Rat Brain in Stereotaxic Coordinates*, 4th ed. Academic: New York, NY.
46. Sanganahalli, B.G., Herman, P., Hyder, F., and Kannurpatti, S.S. (2013). Mitochondrial functional state impacts spontaneous neocortical activity and resting state FMRI. PLoS One 8, e63317.
47. Worsley, K.J., Marrett, S., Neelin, P., Vandal, A.C., Friston, K.J., and Evans, A.C. (1996). A unified statistical approach for determining significant signals in images of cerebral activation. Hum. Brain Mapp. 4, 58–73.
48. Basser, P.J., and Jones, D.K. (2002). Diffusion-tensor MRI: theory, experimental design and data analysis—a technical review. NMR Biomed. 15, 456–467.
49. Basser, P.J., and Pierpaoli, C. (1996). Microstructural and physiological features of tissues elucidated by quantitative-diffusion-tensor MRI. J. Magn. Reson. Ser. B 111, 209–219.
50. Chahboune, H., Mishra, A.M., DeSalvo, M.N., Steib, L.H., Pucaro, M., Scheinost, D., Papademetris, X., Fyson, S.J., Lorincz, M.L., Crunelli, V., Hyder, F., and Blumenfeld, H. (2009). DTI abnormalities in anterior corpus callosum of rats with spike-wave epilepsy. Neuroimage 47, 459–466.
51. Kannurpatti, S.S., Sanganahalli, B.G., Herman, P., and Hyder, F. (2015). Role of mitochondrial calcium uptake homeostasis in resting state fMRI brain networks. NMR Biomed. 28, 10.
52. Keightley, M.L., Sinopoli, K.J., Davis, K.D., Mikulis, D.J., Wennberg, R., Tartaglia, M.C., Chen, J.K., and Tator, C.H. (2014). Is there evidence for neurodegenerative change following traumatic brain injury in children and youth? A scoping review. Front. Hum. Neurosci. 8, 139.
53. Stephens, J.A., Salocio, C.E., Gomes, J.P., Nebel, M.D., Mostofsky, S.H., and Sushauer, S.J. (2017). Response inhibition deficits and altered motor network connectivity in the chronic phase of pediatric traumatic brain injury. J. Neurotrauma 34, 3117–3123.
54. Dona, O., Noseworthy, M.D., DeMatteo, C., and Connolly, J.F. (2017). Fractal analysis of brain blood oxygenation level dependent (BOLD) signals from children with mild traumatic brain injury (mTBI). PLoS One 12, :e0169647.
55. Slobounov, S.M., Gay, M., Zhang, K., Johnson, B., Pennell, D., Sebastionelli, W., Horovitz, S., and Hallett, M. (2011). Alteration of brain functional network at rest and in response to YMCA physical stress test in concussed athletes: RsFMRI study. Neuroimage 55, 1716–1727.
56. Kochanek, P.M., Hendrich, K.S., Dixon, C.E., Schiding, J.K., Williams, D.S., and Ho, C. (2002). Cerebral blood flow at one year after controlled cortical impact in rats: assessment by magnetic resonance imaging. J. Neurotrauma 19, 1029–1037.
57. Giza, C.C., and Hovda, D.A. (2001). The neurometabolic cascade of concussion. J. Athl. Train. 36, 228–235.
58. Hayward, N.M., Immonen, R., Tuuaneu, P.L., Ndode-Ekane, X.E., Grohn, O., and Pitkanen, A. (2010). Association of chronic vascular changes with functional outcome after traumatic brain injury in rats. J. Neurotrauma 27, 2203–2219.
59. Ragan, D.K., McKinstry, R., Benzinger, T., Leonard, J.R., and Pineda, J.A. (2013). Alterations in cerebral oxygen metabolism after traumatic brain injury in children. J. Cereb. Blood Flow Metab. 33, 48–52.

Address correspondence to:
Sridhar S. Kannurpatti, PhD
Department of Radiology
Rutgers–New Jersey Medical School
ADMC-5 Room 575
30 Bergen Street
Newark, NJ 07103

E-mail: kannursr@njms.rutgers.edu